Title:

Genesis of bursting activity: Role of inhibitory constraints on persistent Na+ currents

Abbreviated title:

Plateau generation

Author names and affiliations:

Curtis L. Neveu[1], Douglas A. Baxter[1,2], and John H. Byrne[1]

[1] Department of Neurobiology and Anatomy, W.M. Keck Center for the Neurobiology of Learning and Memory, McGovern Medical School at the University of Texas Health Science Center, Houston, TX 77030.
[2] Engineering Medicine (ENMED), Texas A&M University College of Medicine, Houston, TX 77030.

Corresponding author:

John H. Byrne, Ph.D.

E-mail: John.H.Byrne@uth.tmc.edu

Conflict of interest statement: The authors declare no competing interests.

SUMMARY

Some neurons express a plateau of spike activity greatly outlasting a stimulus, whereas others do not. This difference could be due to differential expression of ion channels (e.g., persistent Na$^+$, and Ca^{2+}) or similar expression of channels that differ in their properties. We compared three *Aplysia* neurons with varying capacity to generate plateau potentials: B51 with self-terminating plateaus, B64 with plateau potentials that do not self-terminate, and the regular spiking neuron B8. Our results indicate the three neurons expressed outward currents I_A and I_D, voltage-gated Ca^{2+} currents I_{CaL} and I_{CaR}, and persistent inward I_{NaP}. The most notable difference observed was a larger I_A, I_D, and I_{KCa} currents in B8, and the plateau generating B64 did not express I_{KCa}. Computational models suggest outward currents suppress and temporally constrain the plateau potential and that inward Ca^{2+} currents suppress plateau potentials when coupled with I_{KCa}.

INTRODUCTION

The relatively simple combination of a fast inward current and a delayed outward current can in principle produce regular neuronal spiking activity where the frequency and duration of firing is directly related to the magnitude and duration of the current stimulus (Canavier et al., 1994). However, many neurons exhibit a more nonlinear burst firing pattern driven by all-or-nothing plateau potentials, causing neurons to fire all-or-nothing bursts of activity, the duration of which can greatly outlast the stimulus (Canavier et al., 1991, 1993, 1994; Nargeot et al., 1999a,b; Plummer and Kirk, 2016). The plateau potential has increasingly become recognized as an important neurophysiological property and has been implicated in many processes such as learning and memory, hippocampal spatial learning, decision making, and rhythmic pattern generation (Bittner et al., 2017) as well as pathological conditions such as epilepsy (Stafstrom 2007; Wengert and Patel 2021). For example, plateau potentials are present in mammalian pyramidal (Bittner et al., 2017), striatal spiny projection (Carrillo-Reid et al., 2009; Plotkin et al., 2011), PreBötC respiratory (Del Negro et al., 2002), and dorsal horn neurons (Derjean et al., 2003) as well as invertebrate neurons including those from the *Aplysia* buccal ganglia (Canavier et al., 1991, 1993, 1994; Nargeot et al., 1999a,b; Plummer and Kirk, 2016). The underlying current thought to mediate many examples of plateau potentials is a persistent Na$^+$ current called (I_{NaP}) (for example see Carrillo-Reid et al., 2009) because this current has a low activation threshold, rapid activation, and a slow inactivation, but the details of this effect still remain an open question. For example, Is I_{NaP} present in all plateau generating neurons? Can other inward currents such as voltage-gated Ca^{2+} currents generate plateau potentials? How do outward currents such as Ca^{2+}-activated

K^+ (I_{KCa}), delayed K^+ (I_D) or A-type K^+ (I_A) channels help determine whether neurons exhibit plateau potentials?

Another question is that of complexity. Are neurons constituted parsimoniously such that regular spiking neurons contain a smaller repertoire of ion channels than plateau-generating neurons? Interestingly, I_{NaP} is not restricted to plateau-generating neurons. Several examples of regular firing neurons have I_{NaP} (Katz et al., 2018). This finding raises the question of what constrains plateau potentials and bursting activity in regular spiking neurons. Plateau-generating neurons could contain the same array of channels as regular spiking neurons, but with different properties to orchestrate plateau potentials. Although less parsimonious, containing the same array of channels with different properties could provide a neuron with greater degrees of freedom and more flexibility to adapt to different circumstances such as in learning.

The neurons in the *Aplysia* feeding system are ideal to identify the important neuronal features dictating regular spiking and plateau-generating activity patterns. Several examples of both types of neurons are present in *Aplysia*. The variety of plateau-generating neurons allows for comparisons within the same neuronal circuit. Moreover, neurons with specific firing properties can be isolated in cell culture and retain their phenotypic behavior (Lorenzetti et al., 2008; Mozziochiodi et al., 2002; Yuto et al., 2022). Here, we examined three isolated neurons in *Aplysia* that vary in their propensity to generate plateau potentials. We then characterized the major membrane currents of these neurons using two-electrode voltage clamp and pharmacologic isolation.

RESULTS

Neurons B51, B64, and B8 vary in their ability to generate plateau potentials.

To investigate the ionic mechanisms of plateau potentials, three neurons were chosen that differ in their ability to generate plateau potentials. The B51 neuron generates a plateau potential that self-terminates after 10 – 20 s (Fig. 1A). B64 generates a plateau potential that does not self-terminate (Fig. 1A), and B8 is a regular spiking neuron unable to generate a plateau potential regardless of the amount of current injected (Fig 1A). We sought to investigate whether different ion channels mediate plateau potentials in B51 and B64 and whether these channels are more similar to each other than they are to the regular firing neuron B8? To investigate this issue, these neurons were isolated from the buccal ganglia (Fig. 1B), maintained in culture and analyzed with two-electrode voltage clamp techniques (Fig. 1C). There were noticeable differences in the morphology of cultured B51, B64 and B8 neurons (Fig. 1D).
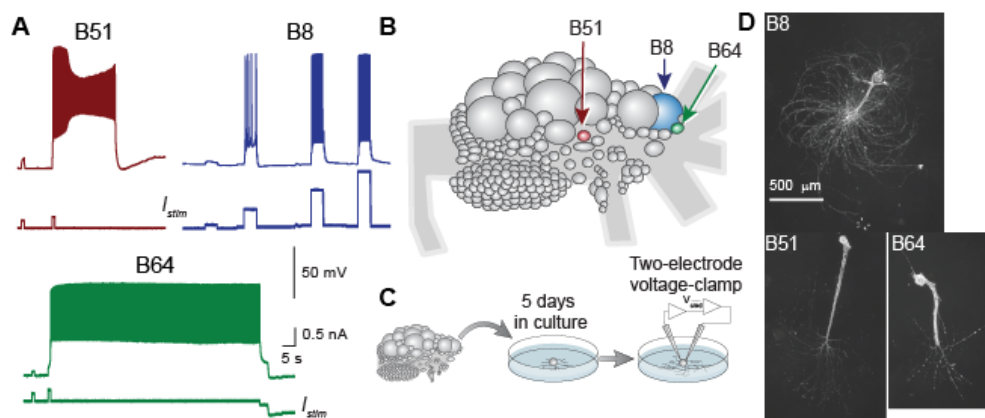
Figure 1. Physiological properties of bursting and pacemaker neurons
(A) Firing properties of neurons B51, B64 and B8. Activity was elicited by 1 s-duration intracellular current injection in B51 and B64, and with a 5 s-duration current injection in B8 because the large membrane time constant in this neuron.
(B) Diagram of rostral surface of buccal ganglion. Neurons were identified by size and position.

(C) Neurons were isolated and recorded by two electrode voltage clamp after 5 – 6 days in culture.

(D) Images of cultured B51, B64, and B8 neurons.

Outward currents of bursting and regular firing neurons

We began our analysis by characterizing the fast activating, fast inactivating I_A, the relatively slower activating and inactivating I_D, and the Ca^{2+} activated I_{KCa}, which are well known to regulate action potential repolarization (for example see Carrasquillo et al., 2012; Newkirk et al., 2021; Yuan et al., 2005).

I_A. I_A was isolated using the selective antagonist 4-aminopyridine (4-AP) (see methods). The maximum conductance g_{max} of I_A was larger in B8 compared to B51 and B64 (B51 = $1.02_{(0.69,\ 1.1)}$ μS, B64 = $0.53_{(0.51,0.54)}$ μS, B8 = $2.6_{(1.8,3.1)}$ μS) (median$_{(25th,75th)}$) ($F_{(2,13)}$ = 23.7, P = 0.0001; *Post hoc*, B51 vs. B64, P = 0.36; B51 vs. B8, P = $7.2x10^{-4}$; B64 vs. B8, P = $1.4x10^{-4}$) suggesting a role of I_A in suppressing plateau potentials. We then examined the slope parameter and halfway point (half-activation, half-inactivation) of the I_A steady-state voltage-gating (Eq. 12). The half-activation of I_A in B51 is shifted to more hyperpolarized potentials compared to B64 and B8 (B51 = $-26.7_{(-28.7,\ -25.0)}$ mV, B64 = $-10.5_{(-13.1,\ -6.7)}$ mV, B8 = $-2.5_{(-11.8,\ -0.72)}$ mV) ($F_{(2,13)}$ = 22.5, P = 0.0001; *Post hoc*, B51 vs. B64, P = 0.0014; B51 vs. B8, P = 0.00014; B64 vs. B8, P = 0.50). The half-inactivation of I_A was also shifted to more hyperpolarized potentials in B51 compared to B64 and B8 (B51 = $-55.8_{(-59.4,\ -55.8)}$ mV, B64 = $-46.3_{(-52.4,\ -44.5)}$ mV, B8 = $-51.0_{(-51.8,\ -45.9)}$ mV) ($F_{(2,13)}$ = 5.94, P = 0.018; *Post hoc*, B51 vs. B64, P = 0.029; B51 vs. B8, P = 0.036; B64 vs. B8, P = 0.95). The inactivation slope parameter (Eq. 15) had a lower absolute value (corresponding to a steeper slope) in B51 compared to B8 (B51 = $-4.3_{(-5.0,\ -3.9)}$, B64 = $-7.4_{(-8.1,\ -6.5)}$, B8 = $-9.4_{(-12.2,\ -7.4)}$) ($F_{(2,13)}$ = 10.4, P = 0.0029; *Post hoc*, B51 vs. B64, P = 0.082; B51 vs. B8, P =

0.002; B64 vs. B8, P = 0.19). There was a trend in a difference in the activation slope parameter (Eq. 12) between the neurons (B51 = $5.6_{(4.6,\ 10.7)}$, B64 = $11.2_{(10.6,\ 13.3)}$, B8 = $10.1_{(9.7,\ 11.7)}$) ($F_{(2,13)}$ = 3.18, P = 0.081). For B51, the leftward shift and steeper slope in the inactivation curve would lead to complete inactivation of I_A during the plateau. Depending on the characteristics of I_D and I_{KCa}, the inactivation of I_A may depolarize the neuron, leading to greater activation of slower outward currents that ultimately terminate B51's plateau. Additionally, the greater g_{max} of I_A in B8 could help prevent any plateau (see below). This greater g_{max} in I_A and the other channels can be explained by the larger size in B8 (Fig. 1 and S4). We investigated the role of morphology in plateau generation and discuss those results in a later section (see below).

I_D. Together with I_A, properties of this current could potentially explain differences in plateau potential generation between B51, B64, and B8. B8 had a larger g_{max} of I_D compared to B51, and B64 tended to have a larger g_{max} compared to B51 (B51 = $1.6_{(1.2,\ 2.0)}$ µS, B64 = $2.9_{(2.3,\ 3.5)}$ µS, B8 = $3.5_{(3.3,\ 4.1)}$ µS) ($F_{(2,14)}$ = 9.19, P = 0.0038; *Post hoc*, B51 vs. B64, P = 0.033; B51 vs. B8, P = 0.0034; B64 vs. B8, P = 0.43). The half-activation was not different between the three neurons (B51 = $-5.0_{(-6.7,\ -3.0)}$ mV, B64 = $-9.4_{(-10.6,\ -3.1)}$ mV, B8 = $-5.9_{(-8.9,\ -2.8)}$ mV) ($F_{(2,14)}$ = 0.31, P = 0.74). The slope of activation was not different between the three neurons (B51 = $9.0_{(8.3,\ 9.1)}$, B64 = $9.2_{(7.3,\ 9.9)}$, B8 = $8.6_{(7.4,\ 9.5)}$) ($F_{(2,14)}$ = 0.07, P = 0.93). I_D did not completely inactivate for all tested command potentials. The maximum level of inactivation was compared between neurons and found to be significantly greater (lower levels of B in Eq. 15) for B8 compared to B64 (B51 = $0.36_{(0.29,\ 0.42)}$, B64 = $0.40_{(0.37,\ 0.44)}$, B8 = $0.27_{(0.26,\ 0.31)}$) ($F_{(2,14)}$ = 5.43, P = 0.021; *Post hoc*, B51 vs. B64, P = 0.33; B51 vs. B8, P = 0.21; B64 vs. B8, P = 0.016). There was no significant

difference in the half-inactivation (B51 = -10.5$_{(-16.9, -9.3)}$ mV, B64 = -10.6$_{(-12.2, -2.7)}$ mV, B8 = -13.4$_{(-15.4, -9.4)}$ mV) ($F_{(2,14)}$ = 1.57, P = 0.25) or inactivation slope (B51 = -4.5$_{(-4.8, -4.4)}$, B64 = = -4.5$_{(-4.8, -4.4)}$, B8 = -5.7$_{(-5.8, -5.4)}$) ($H_{(2)}$ = 5.42, P = 0.067). These data indicate that I_D can be activated by action potentials without being inactivated by the sustained depolarization of the plateau, and thus I_D can possibly affect the duration of the plateau. Additionally, the larger g_{max} of I_D in B8 could prevent the initiation of plateau potentials.
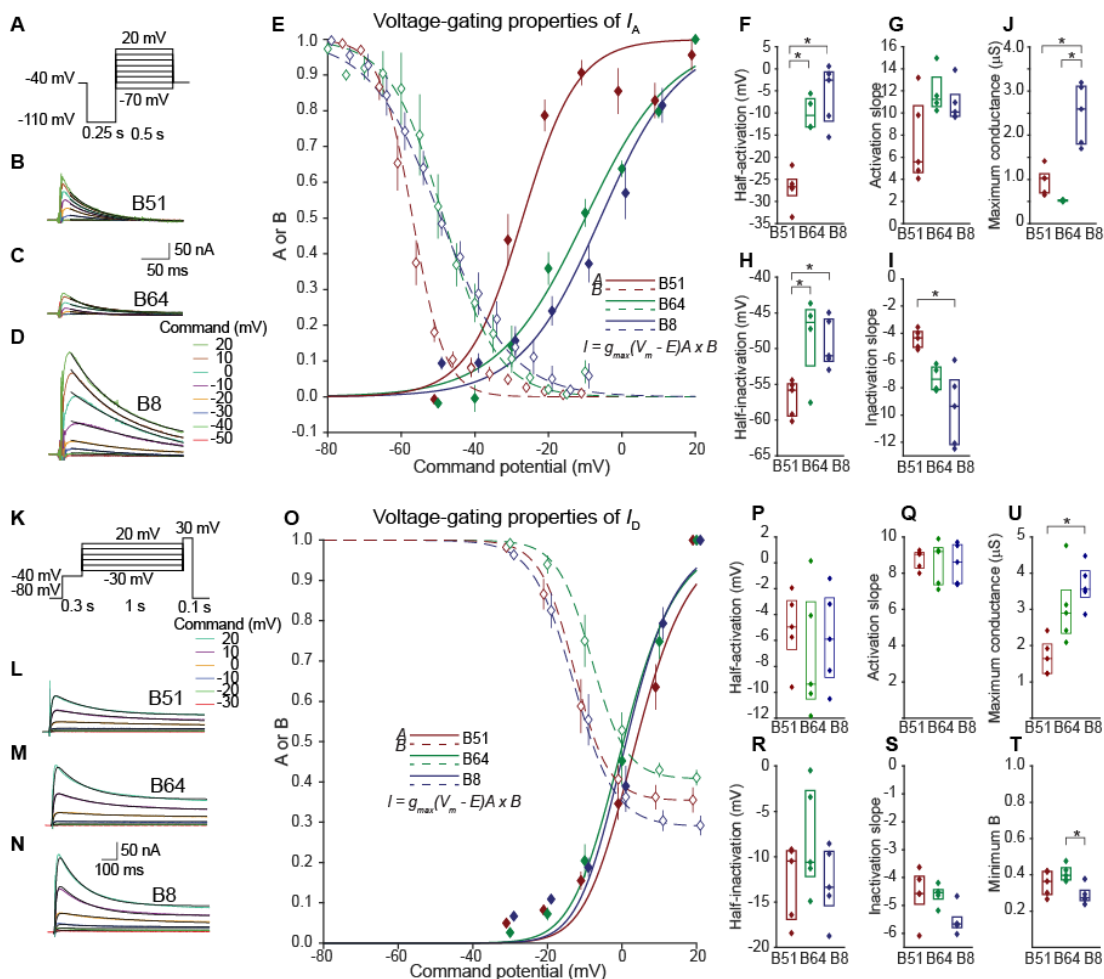
Figure 2. In the plateau-generating neuron B51, I_A and I_D have decreased conductances and leftward shifts in both activation and inactivation curves, as compared to the regular firing neuron B8.

(A) Voltage-clamp protocol to measure I_A. A 250 ms hyperpolarizing prepulse was used to de-inactivate I_A. 4-AP was used to block I_A (see Methods). Inactivation of I_A was measured by a separate voltage clamp protocol (Fig. S1).

(B – D) 4-AP subtracted current response indicating I_A for B51 (B), B64 (C) and B8 (D) for each command potential. A single exponential equation (Eq. 1) was fitted to a 200 ms region beginning 25 ms after start of the command pulse (black line).

(E) Summary data for the inactivation (dashed line, open diamonds) and activation curves (solid line, solid diamond). The data were fit with a Boltzmann equations (Eqs. 12 and 15) with minimum A and B (minimum activation and maximum inactivation) set to 0. Data are represented as box plots. Lower and upper rectangle boundaries are the 25th and 75th percentile and the horizontal line is the median.

(F – I) Summary data for the maximum conductance (Eq. 7) half-activation, activation slope, half inactivation, and inactivation slope parameters of the Boltzmann equations (Eqs. 12 and 15). Data is represented by a boxplot, median is a horizontal line and the interquartile range is represented by a rectangle.

(J) Maximum conductance of I_A was estimated by extrapolating the fitted exponential curve to the beginning of the pulse and calculating conductance using Ohm's law.

(K) Voltage-clamp protocol to measure I_D. A 300 ms prepulse at -40 mV was given to inactivate and reduce contamination by I_A, making use of the lower threshold of inactivation of I_A. The current responses were measured in 2 mM tetraethylammonium (TEA) to block I_{KCa}. The final 100 ms pulse to 30 mV measured the amount of inactivation.

(L – N) Current response indicating I_D for B51 (L), B64 (M) and B8 (N) for each command potential. The product of two exponential equations (Eq. 2) was fitted to a 1 s region beginning at the start of the command pulse (black line).

(O) Summary data for the inactivation (dashed line, open diamonds) and activation curves (solid line, solid diamond) and fitted Boltzmann equations (Eqs. 12 and 15). Data represented as mean and standard error.

(P – T) Summary data for the parameters of the Boltzmann equations. Data is represented by a boxplot, median is a horizontal line and the interquartile range is represented by a rectangle.

(U) Maximum conductance calculated using Ohm's law.

I_{KCa}. First, we examined the contribution of I_{KCa} to plateau generation by blocking the influx of Ca^{2+} suppressing I_{KCa} activation (Fig. 3A-B). The voltage-gated Ca^{2+} channel blocker Ni^{2+} increased the duration of the plateau potential in B51 (control = $5.5_{(0.0, 11.4)}$ s, Ni^{2+} = $32.0_{(14.4, 65.7)}$ s, *paired t-test, $t_{(7)}$* = 2.882, P = 0.024). Plateaus lasting longer than 80 s were terminated artificially by negative current injection. In some cases, B51 neurons

which did not express a plateau potential in control saline, exhibited a strong plateau potential in the presence of Ni^{2+}. There was no significant correlation in plateau duration before and after treatment with of Ni^{2+} (*Pearson's r* = -0.355, P = 0.38, n = 8). These data suggest that I_{KCa} is present in B51 and provides an inhibitory constraint on plateau potentials. We next sought to characterize I_{KCa} and compare its properties amongst the three neurons. I_{KCa} was found in B51 and B8, but not in B64 (Fig. 3D). As with the other outward currents, B8 had a markedly greater g_{max} compared to B51 (B51 = $3.5_{(1.9, 4.9)}$ μS, B8 = $13.6_{(12.9, 27.5)}$ μS, *t-test*, $t_{(11)}$ = 4.52, P = $8.7x10^{-4}$). There was no statistically significant difference in the half-activation between B51 and B8 (B51 = $4.1_{(-8.9, 8.4)}$ mV, B8 = $-1.7_{(-4.8, 4.9)}$ mV, *t-test*, $t_{(12)}$ = -0.135, P = 0.90). There was also no difference in activation slope between B51 and B8 (B51 = $2.6_{(0.55, 8.0)}$, B8 = $7.9_{(2.6, 10.7)}$, *t-test*, $t_{(12)}$ = 0.576, P = 0.58).
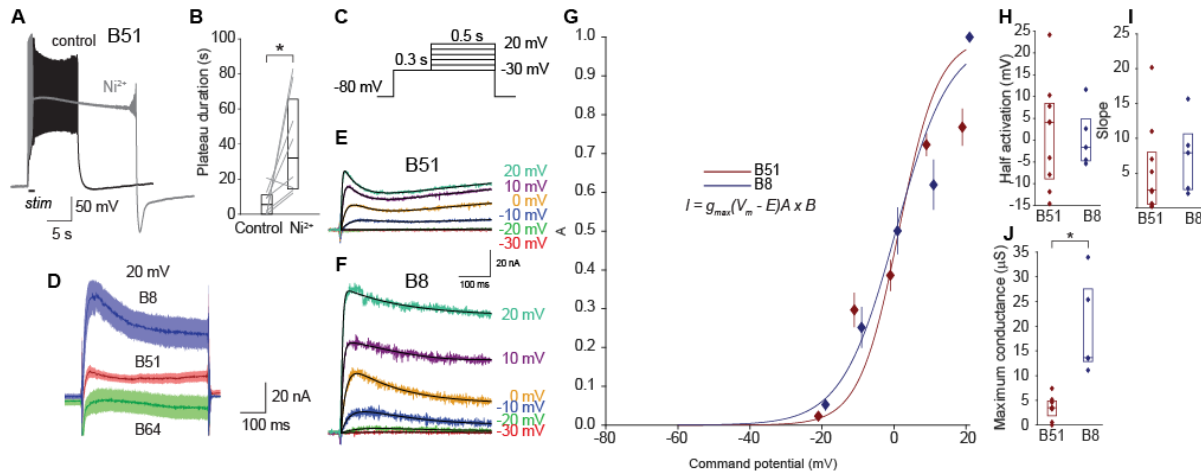
Figure 3. I_{KCa} properties
(A) Example of application of Ni^{2+} increasing the duration of the plateau potential of B51.
(B) Summary data of effects of Ni^{2+} on lengthening the plateau potential of B51. Duration was measured as the amount of time above -70 mV after the end of the stimulus. Data is represented by a boxplot, median is a horizontal line and the interquartile range is represented by a rectangle.

(C) Voltage-clamp protocol to measure I_{KCa}. The current responses in control were subtracted from responses in 2 mM TEA to isolate I_{KCa}.

(D) Summary data for current responses during step to 20 mV. I_{KCa} can be seen for B8 and B51 but not B64.

(E – F) TEA subtracted current response indicating I_{KCa} for B51 (E) and B8 (F) for each command potential. I_{KCa} was not found in B64. The product of three exponentials (activation, inactivation, and slow Ca^{2+} buildup, Eq. 3) was fitted for a 500 ms region beginning 1 ms after the start of the command pulse (black line).

(G) Summary data for the activation curves (solid line, solid diamond) and fitted Boltzmann equations (lines, Eq. 12). Data are represented as mean and standard error.

(H – I) Summary data for the parameters of the Boltzmann equations. Data is represented by a boxplot, median is a horizontal line and the interquartile range is represented by a rectangle.

(J) Maximum conductance calculated using Ohm's law.

Voltage-gated Ca^{2+} channels

Two Ca^{2+} currents, I_{CaL} and I_{CaR}, were characterized.

I_{CaL}. Similar to the outward currents, I_A and I_D, the g_{max} of I_{CaL} was greater in B8 compared to B51 and B64 (B51 = $0.25_{(0.21, 0.28)}$ μS, B64 = $0.17_{(0.17, 0.20)}$ μS, B8 = $0.68_{(0.54, 0.94)}$ μS) ($H_{(2)}$ = 10.26, P = 0.0059; *Post hoc*, B51 vs. B64, P = 0.41; B51 vs. B8, P = 0.14; B64 vs. B8, P = 0.004). The greater conductance could lead to greater influx of Ca^{2+} and greater activation of I_{KCa}, suppressing the plateau potential in B8. There was also a leftward shift of the inactivation curve of B8 compared to B51 (B51 = $-22.2_{(-23.8, -19.2)}$ mV, B64 = $-26.5_{(-27.9, -25.5)}$ mV, B8 = $-34.4_{(-35.7, -30.0)}$ mV) ($H_{(2)}$ = 11.1, P = 0.0040; *Post hoc*, B51 vs. B64, P = 0.18; B51 vs. B8, P = 0.0026; B64 vs. B8, P = 0.27). The difference in inactivation curves would further enhances influx of Ca^{2+} in B8. There were no differences in the half-activation (B51 = $-8.0_{(-12.1, -5.9)}$ mV, B64 = $-4.7_{(-8.0, 0.05)}$ mV, B8 = $-3.7_{(-7.6, -2.5)}$ mV) ($F_{(2,14)}$ = 0.96, P = 0.41), slope of the activation curve (B51 = $7.9_{(3.8, 8.8)}$, B64 = $11.9_{(10.1, 13.0)}$, B8 =

7.9$_{(6.7, 13.0)}$) ($F_{(2,14)}$ = 1.71, P = 0.22), or slope of the inactivation curve (B51 = -0.99$_{(-4.1, -0.91)}$, B64 = -7.5$_{(-7.6, -6.8)}$, B8 = -6.3$_{(-6.6, -6.0)}$) ($H_{(2)}$ = 4.5, P = 0.105).
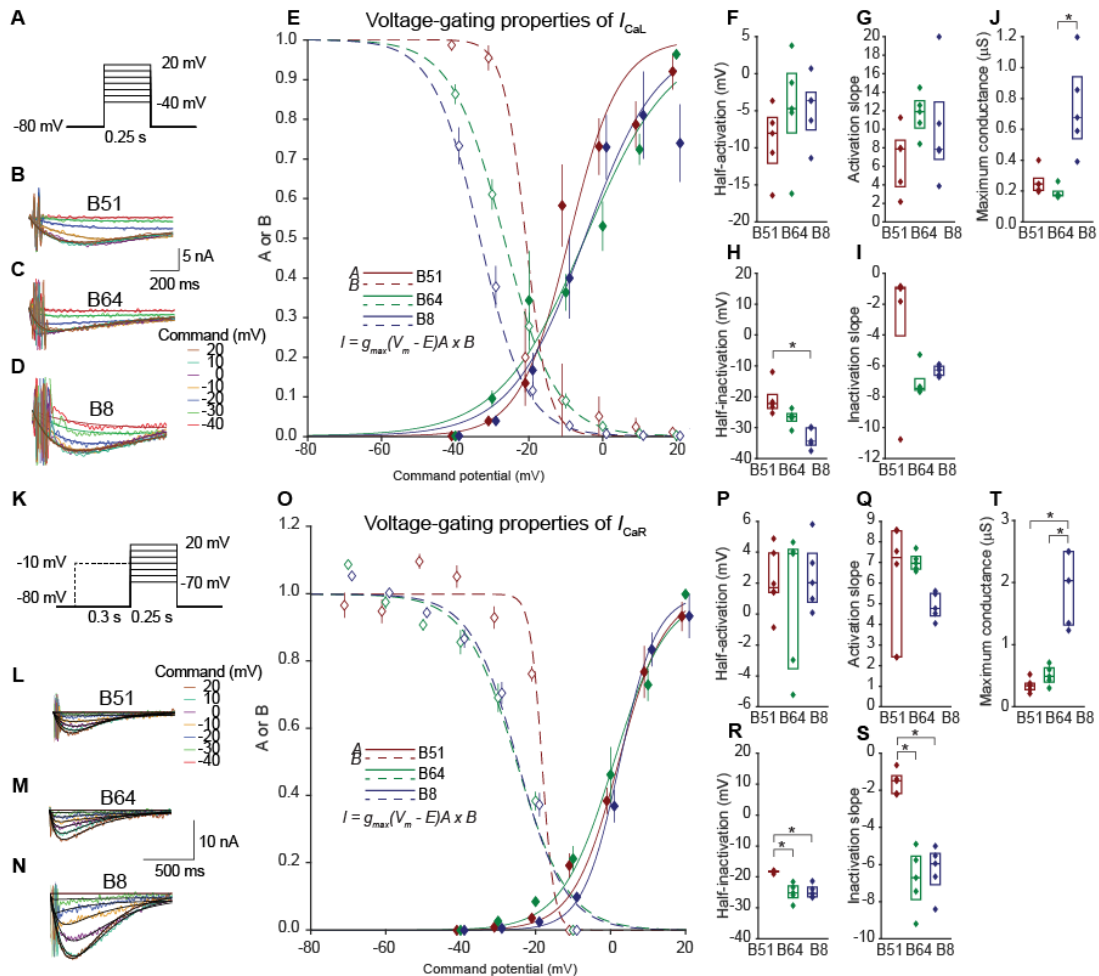
Figure 4. Steady-state properties of I_{CaL} and I_{CaR} indicate greater conductances in the pacemaker neuron B8 and rightward shifts in the activation and inactivation curves of B51.

(A) Voltage-clamp protocol to measure I_{CaL}. The current responses in control were subtracted from responses in 10 μM nifedipine to isolate I_{CaL}. Inactivation for I_{CaL} was measured by a separate voltage clamp protocol (Fig. S2).

(B – D) Subtracted current responses indicating I_{CaL} for B51 (B), B64 (C) and B8 (D) for each command potential. A double exponential equation (Eq. 4) was fitted to a 100 ms region beginning 2 ms after start of the command pulse (black line).

(E) Summary data for the inactivation (dashed line, open diamonds) and activation curves (solid line, solid diamond). The data were fit with a Boltzmann equation (Eqs. 12 and 15) with minimum A and B (minimum activation and maximum inactivation) set to 0. Data are represented as mean and standard error.

(F – I) Summary data for the parameters of the Boltzmann equations. Data is represented by a boxplot, median is a horizontal line and the interquartile range is represented by a rectangle.

(J) Maximum conductance of I_{CaL} was calculated using Ohm's law.

(K) Voltage-clamp protocol to measure I_{CaR}. A 300 ms prepulse at -10 mV was given to inactivate I_{CaR}. Protocols were administered in the presence of nifedipine to block CaL. The current responses without prepulse were subtracted from responses with the prepulse to isolate I_{CaR}. Inactivation for I_{CaR} was measured by a separate voltage clamp protocol (Fig. S2).

(L – N) Subtracted current response indicating I_{CaR} for B51 (A), B64 (B) and B8 (C) for each command potential. A double exponential equation (Eq. 4) was fitted to a 120 ms region beginning 8 ms after the start of the command pulse (black line).

(O) Summary data for the inactivation (dashed line, open diamonds) and activation curves (solid line, solid diamond) and fitted Boltzmann equations (lines, Eqs. 12 and 15). Data represented as mean and standard error.

(P – T) Summary data for the parameters of the Boltzmann equations. Data is represented by a boxplot, median is a horizontal line and the interquartile range is represented by a rectangle.

(U) Maximum conductance calculated using Ohm's law.

I_{CaR}. Similar to I_A, I_D, and I_{CaL}, the g_{max} of I_{CaR} was greater in B8 compared to B51 and B64 (B51 = 0.34$_{(0.28, 0.38)}$ μS, B64 = 0.49$_{(0.40, 0.63)}$ μS, B8 = 2.03$_{(1.32, 2.5)}$ μS) (F$_{(2,14)}$ = 31.0, P = 1.12x10^{-5}; *Post hoc*, B51 vs. B64, P = 0.74; B51 vs. B8, P = 1.61x10^{-5}; B64 vs. B8, P = 7.61x10^{-5}), which could contribute to suppression of the plateau in B8. There was also a rightward shift of the inactivation curve of B51 compared to B64 and B8 (B51 = -18.1$_{(-18.4, -18.1)}$ mV, B64 = -25.1$_{(-26.7, -22.9)}$ mV, B8 = -25.3$_{(-26.4, -23.3)}$ mV) (H$_{(2)}$ = 9.38, P = 0.0092; *Post hoc*, B51 vs. B64, P = 0.024; B51 vs. B8, P = 0.020; B64 vs. B8, P = 0.997) and a steeper slope of the inactivation curve in B51 compared to B64 and B8 (B51 = -1.49$_{(1.21, 2.18)}$, B64 = -6.7$_{(5.54, 7.9)}$, B8 = -5.95$_{(5.39, 7.09)}$) (F$_{(2,14)}$ = 25.5, P = 4.77x10^{-5}; *Post hoc*, B51 vs. B64, P = 8.5x10^{-5}; B51 vs. B8, P = 0.0002; B64 vs. B8, P = 0.82). There

was no significant difference in the half-activation (B51 = $1.7_{(1.4, 3.9)}$ mV, B64 = $3.9_{(-3.5, 4.2)}$ mV, B8 = $2.0_{(0.76, 3.9)}$ mV) ($H_{(2)}$ = 0.04, P = 0.98) or slope of the activation curve between the three neurons (B51 = $7.2_{(2.4, 8.5)}$, B64 = $7.0_{(6.7, 7.3)}$, B8 = $4.8_{(4.4, 5.5)}$) ($F_{(2,15)}$ = 1.67, P = 0.226).

The activation curve of I_{CaR} was shifted to the right compared to I_{CaL} suggesting that I_{CaL} may contribute more to Ca^{2+} influx during the plateau compared to I_{CaR}. Also, it is worth noting that the activation and inactivation curves indicate that these channels are not inactivated at resting potential become active only during neuronal activity.

Persistent Na$^+$ channel

We hypothesized that I_{NaP} is more pronounced in B51 and B64 compared to B8 because of I_{NaP} established role in maintaining sustained depolarizations. As a first step, we sought to identify a pharmacologic agent that could block I_{NaP} without blocking the faster I_{Na}. Therefore, we completed a dose response curve for two compounds suggested to block I_{NaP}, TTX and rilizule. We measured the duration of the plateau potential as an indicator for I_{NaP} and the amplitude of the action potential as an indicator of I_{Na} (Fig. 5A-B). The dose response curve indicated that 10 μM was a reasonable concentration of TTX that blocked approximately 91.2±1.3% of I_{NaP} while only blocking 20.6±0.7% of I_{Na}. A similar experiment with rilizule indicated that 20 μM rilizule blocked 79.5±0.2% of I_{NaP} while only blocking 14.7±0.4% of I_{Na}. However, voltage-clamp experiments with rilizule was not specific to voltage-gated sodium channels, whereas TTX was highly specific to I_{NaP} at 10 μM. Therefore, 10 μM TTX was selected to characterize I_{NaP}. Surprisingly, I_{NaP} was not significantly different among the three neurons. There was no statistical difference in half-activation (B51 = $-47.1_{(-49.9, -38.1)}$ mV, B64 = $-39.5_{(-44.3, -36.0)}$ mV, B8 = $-44.7_{(-50.8, -42.2)}$ mV)

$(F_{(2,24)} = 2.76, P = 0.085)$, slope of the activation curve (B51 = $2.2_{(1.3, 3.3)}$, B64 = $2.4_{(1.9, 5.5)}$, B8 = $2.7_{(1.3, 5.5)}$) $(F_{(2,24)} = 0.39, P = 0.68)$, or g_{max} (B51 = $0.34_{(0.25, 0.39)}$ μS, B64 = $0.23_{(0.16, 0.42)}$ μS, B8 = $0.38_{(0.29, 0.61)}$ μS) $(F_{(2,24)} = 0.87, P = 0.43)$. This indicates that the different propensities to generate plateau potentials amongst B51, B64 and B8 must depend on the outward currents or the voltage-gated Ca^{2+} channels.
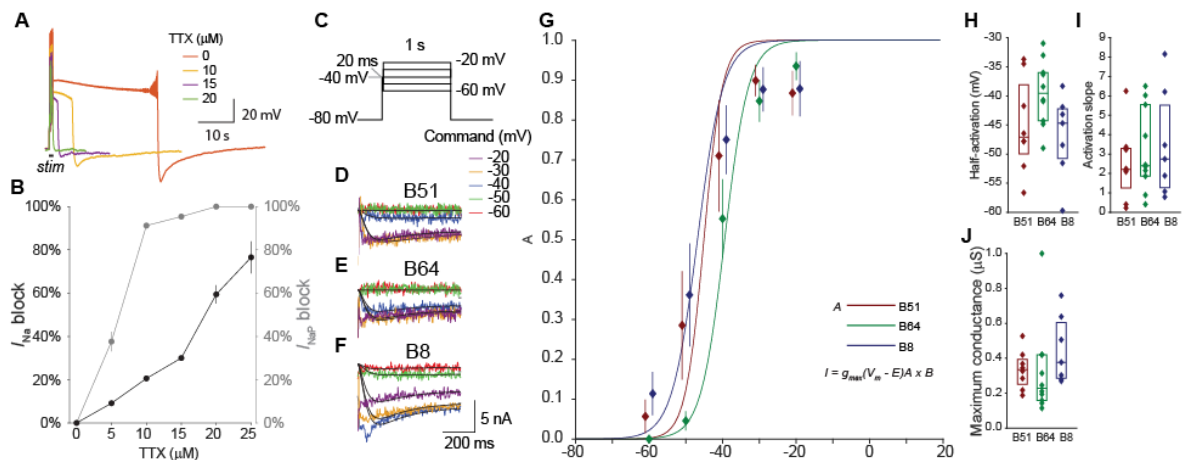
Figure 5. I_{Nap} expressed in both bursting and pacemaker neurons has similar properties

(A) Example neuron showing the reduction in plateau duration by TTX.

(B) Dose response curve of TTX. The block of I_{Na} was measured as the decrease in action potential amplitude, whereas the block of I_{Nap} was measured by the percent decrease in the amount of time above -70 mV after the end of the stimulus.

(C) Voltage-clamp protocol to measure I_{Nap}. A 20 ms step to -40 mV was used to reduce contamination by I_{Na}. The current responses in control were was subtracted from responses in 10 μM TTX to isolate I_{Nap}.

(D – F) TTX subtracted current response indicating I_{Nap} for B51 (D), B64 (E) and B8 (F) for each command potential. A double exponential equation (Eq. 5) was fitted for a 640 ms region beginning 9 ms after the start of the command pulse (black line).

(G) Summary data for the activation curves (solid line, solid diamond) and fitted Boltzmann equations (lines, Eq. 12). Data represented as mean and standard error.

(H – I) Summary data for the parameters of the Boltzmann equations.

(J) Maximum conductance calculated using Ohm's law.

Computational models replicate dynamics of B51, B64, and B8.

A conductance-based model of each neuron was built to investigate the ways in which these channels interact to mediate plateau potentials. For simplicity, we modeled each neuron as a single compartment. A model of each channel was constructed in agreement with the empirically measured voltage-dependency of steady-state activation and inactivation (Figs. 2-5) and estimations of the voltage-dependency of the time constants (Supplementary Fig. 2). The I_{HCN} current was characterized and added to B8 because of its pronounced sag potential and ability to produce rebound excitation in this neuron (Supplementary Fig. 3G). The resultant models reproduced the salient dynamics of each neuron. Specifically, the B51 model expressed a plateau potential that self-terminated, the B64 model expressed a plateau potential that did not self-terminate, and the B8 model did not express a plateau potential for any of the stimuli tested (Fig. 6D).

We next examined the window current, which is calculated using Ohm's law and the product of the steady-state activation and inactivation curves (Eqs. 7, 12, and 15). Each current was normalized to the sum of all of the currents to display the dominant sustained current at each membrane potential (Fig. 6A-C). I_{NaP} was the dominant sustained current at subthreshold potentials and peaks at about -40 mV, suggesting that I_{NaP} mediates sustained depolarization during a plateau potential. However, a more complex set of channels mediate sustained current around -60 mV. At this potential, I_{CaL} seems to dominate in B51 and B64, but the outward current I_{KCa} was greatest at this potential in B8. Outward currents I_D and I_{KCa} dominated the sustained current at potentials more positive than approximately -5 mV, further supporting their role in repolarizing the membrane after an action potential.
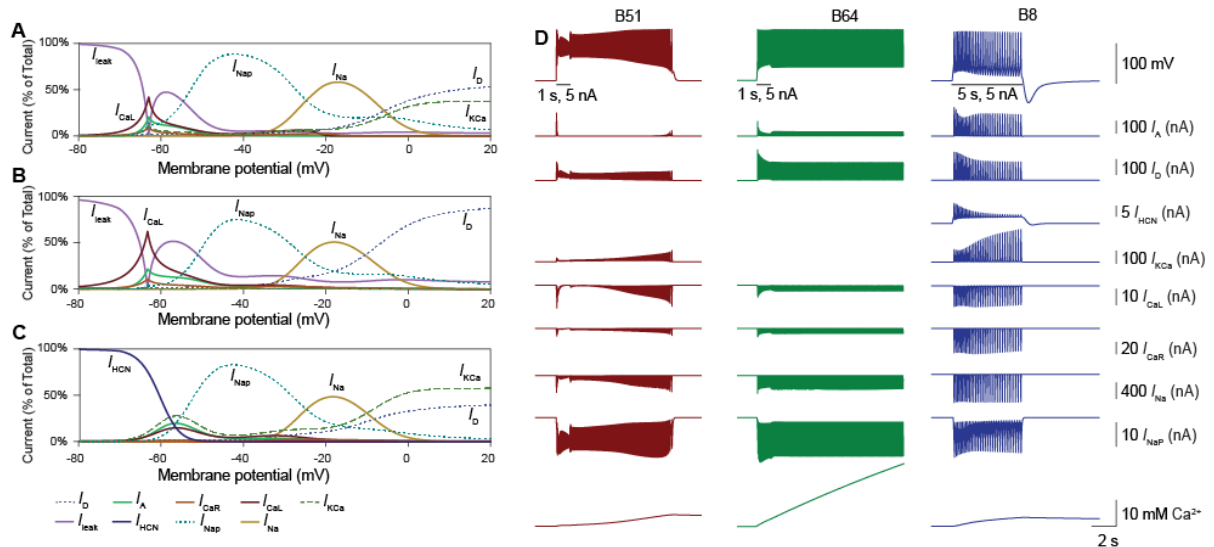
Figure 6. Simulations indicated outward currents I_{KCa}, I_A, and I_D terminated plateau potentials and could suppress the initiation of plateau potentials.

(A – C) Plots showing the dominant steady-state current for each membrane potential. I_{leak} and I_{HCN} dominate at holding potential (-80 mV), I_{NaP} dominates at subthreshold depolarization, I_{Na} dominates at depolarized potentials, I_D and I_{KCa} dominate at depolarized potentials. Currents such as I_A completely inactivate at all potentials so are not observed.

(B) Current responses and Ca^{2+} pool during simulated activity triggered by a 5 nA current injection (1 s for B51 and B64, 5 s for B8). B8 has a pronounced hyperpolarization sag potential. We confirmed the presence of I_{HCN} by Cs$^+$ and ZD7288 and then characterized I_{HCN} in B8 (Supplementary Fig. [not yet added]). I_{HCN} was then substituted it for I_{Leak} in B8.

The dynamic current responses during activation differed between the neuronal models when activated by a simulated depolarizing current injection. I_{NaP} was more prominent in B51 and B64, whereas there were substantially greater amounts of I_A, I_D, I_{KCa}, I_{CaL} and I_{CaR} currents in B8. Any of these currents could potentially lead to the suppression of plateau potentials either directly (i.e., I_A, I_D, I_{KCa}) or indirectly by I_{CaL} and I_{CaR} activation of I_{KCa}. Therefore, we examined which currents more strongly affected the propensity to generate plateau potentials.

Relative contributions of currents to plateau potentials

To investigate how strongly each current affects the propensity to generate plateau potentials, we varied the g_{max} (Eq. 7) of either I_A, I_D, I_{KCa}, I_{CaL}, or I_{CaR} while also varying the g_{max} of I_{NaP} (Fig. 7). Currents that were not being manipulated were kept at their control values. The g_{max} was chosen because this channel property differed the most between the three neurons. The duration of the plateau potential, measured at the end of a sufficiently strong stimulus (5 nA, 1 s simulated current injection), was used to indicate the propensity to generate a plateau potential. Increasing the g_{max} of channels that strongly suppress plateau potentials would require a commensurate increase in the g_{max} of I_{NaP} to maintain the propensity to generate a plateau potential. Conversely, currents that have little effect on plateau potentials would not require additional increases in I_{NaP}. With these manipulations, we found that in B51, I_D, I_{KCa}, and I_{CaL} strongly suppressed the plateau potential whereas I_{CaR} had little effect and I_A had no effect and at all. In contrast, in B64, I_D and I_A both suppressed the plateau potential. This neuron did not have I_{KCa}, so we artificially included the I_{KCa} model used in B8 and varied its g_{max} to test the effect of I_{KCa} on B64 plateau potentials. I_{KCa} strongly suppressed the plateau potential in B64. I_{KCa} was set to zero in B64 when testing the effects of channels other than I_{KCa}. I_{CaR} did not suppress and I_{CaL} slightly facilitated the plateau potential in B64. The B8 model was not prone to generating plateau potentials except when g_{max} of I_{KCa} or I_D was much lower than control values. These results indicate that I_D and I_{KCa} strongly suppress plateau potentials regardless of cell type, however
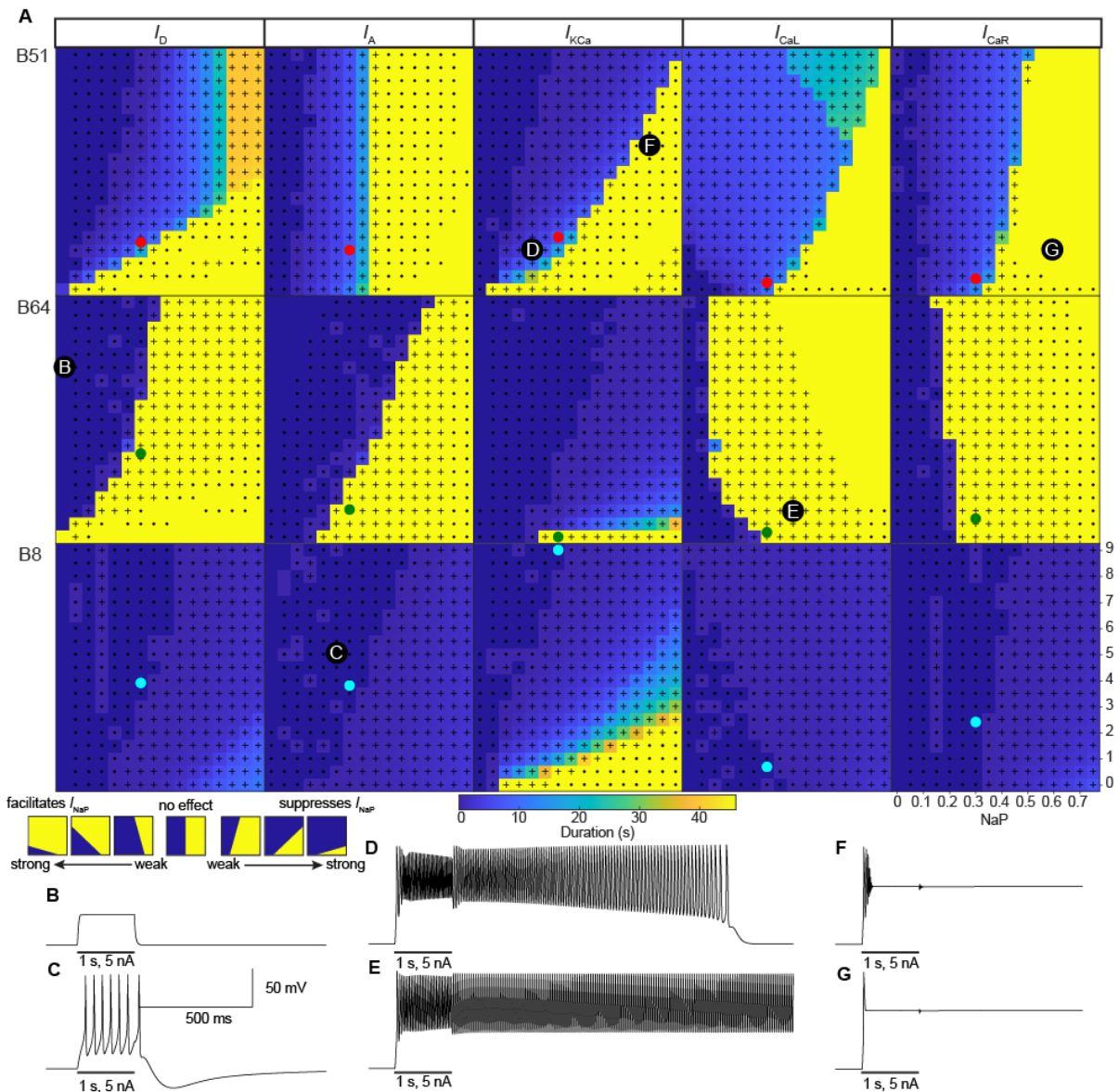
Figure 7. Heat maps of the parameter space indicate that ion channels affect each neuron in different ways.

(A) Heat maps of the effects of varying g_{max} for I_D, I_A, I_{KCa}, I_{CaL}, and I_{CaR} vs. I_{NaP} on the plateau duration. The g_{max} of the outward currents and Ca^{2+} currents were each varied from 0 to 9 μS, while that of I_{NaP} was varied independently from 0 to 0.75 μS. The remaining model parameters were determined by experimental data presented in Figs. 1-5 and Supplemental Figs. 1-3. A guide to interpreting the maps is provided on the bottom left. The neuron model was held to -80 mV, similar to empirical experiments, and activity was elicited by a 1 s, 5 nA simulated positive current injection. The filled circles indicate the default values of g_{max} in the model (red = B51, green = B64, cyan =

B8). The dots indicate a neuron that fires at least 3 action potentials. The + indicates action potentials occurred after the end of the positive current injection.

(B – G) Illustrations of model responses. The g_{max} values for models in B – G are indicated in A.

(B) Example of voltage response in a non-spiking model.

(C) Example of a regular spiking model.

(D) Example of a model with a self-terminating plateau potential.

(E) Example of a spiking model with a plateau potential that does not self-terminate.

(F) Example of a spike deficient model with a plateau that does not self-terminate.

(G) Example of a model unable to elicit spikes with a plateau that does not self-terminate.

I_A and I_{CaL} only suppressed plateau potentials in particular neurons, whereas I_{CaR} had marginal effects on the plateau potential in all three neurons. In addition to plateau duration, we examined the voltage of the plateau potential (measured at the troughs between action potentials) and found that plateau potential heatmaps were visibly similar to plateau duration heatmaps (Supplementary Fig. 5). Interestingly, a heatmap of the action potential duration (Supplementary Fig. 6) had a more complex patterning highlighting the complex relationship between the ionic currents and shape of the action potential.

In addition to examining the voltage-dependent conductances, we also examined the passive properties in cultured B51, B64, and B8 neurons to determine their role in plateau generation. B51 had a significantly greater input resistance than B64 and B8, but B8 had a greater capacitance and membrane time constant than B51 and B64 (Supplementary Fig 4A-C). Modifying the capacitance in these model neurons only had marginal effects on plateau generation indicating that passive properties are unlikely to contribute significantly to the plateau potential (Supplementary Fig 4D).

DISCUSSION

This study comprehensively studied three neurons that varied in their ability to produce the highly nonlinear, all-or-nothing bursting activity mediated by plateau potentials. The results indicate that regular spiking neurons like B8 can be more complex than what might be expected, containing the same conductances as in plateau generating neurons. The main difference among these neurons was greater outward currents and voltage-gated Ca^{2+} currents in B8. Interestingly, all three neurons contained similar properties of I_{NaP}. The similar array of ion channels and increased outward current suggest that plateau potentials result not from additional channels that enable an upper depolarized state, but rather a release of inhibitory constraints like I_D and I_{KCa}.

Similarity of *Aplysia* channels with other systems

The steady-state activation and inactivation properties of each channel had remarkable similarity to their counterparts in mammalian systems. For example, the activation and inactivation curves of I_D agree with measurements in *X. laevis* (Tsuk et al. 2005), and I_{CaL} agrees with measurements of human I_{CaL} expressed in HEK cells (Jangsangthong et al., 2010). For I_{CaR}, the activation curve closely matched I_{CaR} in cerebellar granule cells, however the I_{CaR} inactivation curve in *Aplysia* was shifted to the right by 20 mV compared to I_{CaR} in these granule cells (Randall and Tsien, 1997). In this case, I_{CaR} would be more effective in regulating the plateau potential in granule cells than it is in *Aplysia*.

Voltage-gated Ca^{2+} channel's involvement in plateau generation

The results from the current study suggest that I_{CaL} suppressed plateau potentials in neurons that expressed I_{KCa} whereas I_{CaR} had less of an effect on plateau potentials. In barrelette cells, blocking I_{CaL} also blocks plateau potentials (Lo and Erzurumlu 2002). In

addition, Ni^{2+} blocked bursting in hippocampal neurons suggesting a possible role of I_{CaR} in plateau generation in these neurons (Metz et al., 2005). The results in barrelette and hippocampal neurons could be explained by I_{KCa} either not being expressed sufficiently in these neurons or being expressed in a different cellular region. Another possibility is that these voltage-gated Ca^{2+} channels enhance excitatory input and this enhanced input facilitates plateau generation. This study did not investigate the T-type Ca^{2+} channel (I_{CaT}), which has also been implicated in bursting activity (Broicher et. al., 2007). The lower threshold of I_{CaT} would enable this current to play a larger role in plateau initiation, however the lower inactivation threshold would likely inactivate I_{CaT} for the majority of the plateau. It would be interesting to compare I_{CaT} role in plateau potentials in B51 or B64 in future studies.

I_A, I_D and I_{KCa} involvement in plateau generation

This study found that the outward currents I_A, I_D and I_{KCa} regulated plateau potentials. The strongest regulator of plateau potentials was I_{KCa}. In the mouse pituitary, the Ca^{2+}-activated channels IK and BK had opposing effects on bursting. Inhibition of IK enhanced whereas inhibition of BK decreased bursting activity (for review see Duncan and Shipston, 2016). The delayed rectifier K^+ has also been implicated in regulating burst firing. For example, a Kv2 blocker, guangxitoxin-1E, increased bursting in layer 5 pyramidal neurons (Newkirk et al., 2021).

I_{NaP} involvement in plateau generation

This study brings additional experimental and computational support for the important role of I_{NaP} in mediating the plateau potential. Similar to previous studies, our results indicated that I_{NaP} does not fully inactivate and is activated at subthreshold voltages (Pennartz et

al., 1997). In addition, computational models indicate that increasing I_{NaP} leads to plateau potentials.

STAR METHODS

RESOURCE AVAILABILITY

Lead contact

Further information and requests for resources and reagents should be directed to and will be fulfilled by the lead contact, John H. Byrne (John.H.Byrne@uth.tmc.edu).

Materials availability

No new materials were created in this study.

Data and code availability

- Raw data and annotated spreadsheets are deposited on Google Drive. A link will be provided on request.

- The code for mathematical simulation is provided on ModelDB. The analysis routines were written in MATLAB are provided on GitHub at http:abc.com.

- Any additional information for reanalyzing the data is available from the Lead Contact upon request.

EXPERIMENTAL MODEL AND SUBJECT DETAILS

Animals

Aplysia californica (100 – 120 g) were obtained from the National Resource for *Aplysia* (University of Miami, FL). Animals were housed in perforated plastic cages in aerated seawater tanks at a temperature of 15 °C and were fed ~1 g of dried seaweed three times per week.

Cell culture

Culturing procedures followed those described in Brembs et al. (2002) and Lorenzetti et al. (2008). Briefly, ganglia from adult *Aplysia* were treated with Dispase® II (9.4 units/ml) (neutral protease, grade II) (Roche, Indianapolis, IL) at 35°C for ~3 h and then desheathed. Fine-tipped glass microelectrodes were used to remove individual cells from the ganglia. Each cell was isolated and plated on poly-L-lysine (0.75 mg/ml) coated petri dishes with culture medium containing 50% hemolymph, 50% isotonic L15 (Invitrogen, Carlsbad, CA). L15 was made of 350 mM NaCl, 29 mM $MgCl_2$, 25 mM $MgSO_4$, 11.4 mM $CaCl_2$, 10 mM KCl, 2 mM HCO_3, streptomycin sulfate (0.10 mg/mL), penicillin-G (0.10 mg/mL), dextrose (6 mg/mL) and 15 mM HEPES. The pH of the culture medium was adjusted to 7.5. Cells were maintained for 5-6 days. Prior to recording, the culture medium was exchanged for isotonic ASW solution containing 425 mM NaCl, 12.5 mM $MgSO_4$, 11.2 mM $CaCl_2$, 42 mM $MgCl_2$, 10 mM KCl, and 12.5 mM HEPES (pH 7.6 titrated with NaOH). In cases where voltage or Ca^{2+}-gated K^+-channels were examined N-methyl-D-glucamine (NMDG) substituted Na^+ (425 mM). The NMDG substituted ASW (nASW) was titrated with HCl.

Intracellular recordings

Intracellular recordings were performed at room temperature (20-22ºC) using two fine-tipped glass microelectrodes filled with 3M potassium acetate (resistance 7-15 MΩ). One electrode was used for monitoring membrane potential and a second for injecting current. Signals were amplified using the Axoclamp-2B (Molecular Devices, Sunnyvale, CA). The holding current was passed through an AAA amplifier prior to digitization. Data were acquired at 5-10 kHz with pClamp (Version 11, Molecular Devices, Sunnyvale, CA)

software and filtered with a lowpass filter using Matlab with the cutoff between 300 – 700 Hz.

Whole-cell two-electrode voltage-clamp and pharmacological techniques were used to examine the properties of voltage-gated ion channels. The voltage-clamp protocol was modified to best isolate each conductance. The pharmacological agents were dissolved in 15 mL (~5x bath volume) and perfused at a rate of 2 mL/min. For the A-type K^+ (I_A), the membrane potential was held at -40 mV, stepped to -110 mV for 250 ms to de-inactivate the I_A, then immediately stepped to potentials ranging from -50 mV to 20 mV for 500 ms. The interval between each voltage-clamp stimulus (interstimulus interval, ISI) was set to 4 s. This protocol was carried out in two conditions: 200 μM 4-aminopyridine (4-AP) a concentration that does not block I_A and in 10 mM 4-AP, a concentration that inhibits I_A. The low concentration of 200 μM 4-AP was chosen to reduce contamination of I_{KCa}. Both cases used nASW containing 10 mM Ni^{2+} and 100 μM Cd^{2+} to block voltage-gated Ca^{2+} channels and I_{KCa}. The current responses during the two pharmacological conditions were subtracted to isolate I_A. For the delayed K^+ channel (I_D), the membrane potential was held at -80 mV, stepped to -40 mV for 300 ms to inactivate I_A, then immediately stepped to potentials ranging from -30 mV to 20 mV for 1 s. The ISI was set to 60 s. I_D was measured in nASW containing 2 mM tetraethylammonium (TEA) and 10 mM Ni^{2+} and 100 μM Cd^{2+} to block I_{KCa} and voltage-gated Ca^{2+} channels. For I_{KCa}, the membrane potential was held at -80 mV, stepped to -30 mV for 300 ms to inactivate I_A, then immediately stepped to potentials ranging from -30 mV to 20 mV for 500 ms. The ISI was set to 3 s. This protocol was carried out in control nASW and nASW containing 2 mM TEA, a concentration that selectively inhibits

I_{KCa} (Baxter and Byrne, 1989). The current responses during the two pharmacological conditions were subtracted to isolated I_{KCa}. For the L-type Ca^{2+} channel (I_{CaL}), the membrane potential was held at -80 mV and stepped to potentials ranging from -40 mV to 20 mV for 250 ms. The ISI was 30 s. This protocol was repeated in control nASW and nASW containing the I_{CaL} inhibitor nifedipine (10 μM). Both conditions contained 10 mM 4-AP and 50 mM TEA to block I_A, I_D, and I_{KCa}. The current responses during the two pharmacological conditions were subtracted to isolate I_{CaL}. For the R-type Ca^{2+} channel (I_{CaR}), the membrane potential was held at -80 mV and stepped to potentials ranging from -40 mV to 20 mV for 250 ms. The ISI was set to 30 s. This protocol was repeated with a 300 ms prepulse to -10 mV to inactivate the I_{CaR}. Both protocols were done in the presence of nASW containing 10 μM nifedipine, 10 mM 4-AP and 50 mM TEA to block I_{CaL}, I_A, I_D, and I_{KCa}. The current responses elicited by the protocol without the prepulse were subtracted from the current responses with the prepulse to isolated I_{CaR}. For the persistent Na^+ (I_{NaP}), the membrane potential was held at -100 mV, stepped to -40 mV for 20 ms to inactivate the $I_{Na,fast}$ channel, then immediately stepped to potentials ranging from -60 mV to -20 mV for 1 s. The ISI was set to 30 s. This protocol was repeated in ASW containing the voltage-gated Na^+ inhibitor tetrodotoxin (10 μM TTX). The current responses during the two pharmacological conditions were subtracted to isolate I_{NaP}.

Fitting equations to current responses

All automated curve fitting was done by the built-in MATLAB function lsqcurvefit using the default 'trust-region-reflective' or the Levenberg-Marquardt least squares algorithms. I_A current traces were fit with the following single-exponential equation:

$$f(t) = Ae^{\frac{-t}{s}} + b \tag{1}$$

where A is a positive value representing the amplitude of the current, s is the time constant of inactivation and b is a baseline offset. This curve was fitted to a 200 ms region starting 25 ms after the start of the pulse for each command potential. The curve was extrapolated backwards 25 ms to obtain the initial current at the start of the pulse.

I_D current traces were fit with the following double-exponential equation:

$$f(t) = A\left(1 - e^{\frac{-t}{0.01}}\right)\left(1 - B\left(1 - e^{\frac{-t}{s}}\right)\right) \tag{2}$$

where the parameter A is the maximum current and is a value limited to between 1 and 1.5 times the peak of the current trace. The peak for I_D was estimated by taking the 99th percentile of the current trace. To reduce the number of fitting parameters, the activation time constant was fixed at 0.01 s, a value which provided the best fit for the data. The parameter s is the time constant of inactivation limited to a value greater than 0.16 s. B is the amount of inactivation and was determined by a voltage step to 30 mV following a 1 s step to various potentials (Fig. 2K and Supplemental Fig. 1B). The second term of Eq. 2-4 is equal to B_∞ in Eq. 15 when time is carried out to infinity. The current response measured at 18.7 ms after the start of the 30 mV pulse was normalized to the current measured with the prepulse that resulted in no inactivation (-30 mV). As for I_A, I_{CaL}, and I_{CaR} the inactivation data were fit with Eq. 5. The values returned from the fitted equation are inserted for B in Eq. 2.

I_{KCa} current traces were fit with the following triple exponential equation:

$$f(t) = A\left(1 - e^{\frac{-t}{s_1}}\right)\left(1 - B\left(1 - e^{\frac{-t}{s_2}}\right)\right)\left(0.1 + C(1 - e^{-t})\right) \tag{3}$$

where A is limited to a positive value. B is limited to between 0 and 1. For Eq. 3, B was not directly measured using a separate voltage-clamp protocol. The parameters s_1 and s_2 are the activation and inactivation time constants respectively. The third term of Eq. 3 describes the regulation of the I_{KCa} by Ca^{2+}. The value 0.1 is the initial value. The parameter C is the value of Ca^{2+} saturation.

I_{CaL} and I_{CaR} current traces were fit with the following double-exponential equation:

$$f(t) = A\left(1 - e^{\frac{-t}{s_1}}\right)\left(1 - B\left(1 - e^{\frac{-t}{s_2}}\right)\right) \tag{4}$$

where A is the maximum current and limited to a value between -100 and 0 nA, which exceeded the largest current measured for these channels. s_1 is the activation time constant and limited to between 0.002–0.05 s for I_{CaL} and 0.001–0.05 s for I_{CaR}, s_2 is the inactivation time constant and limited to between 0.02–0.5 s for I_{CaL} and 0.025–0.5 s for I_{CaR}. B is the amount of inactivation and was measured by a separate voltage clamp protocol. A 1 s prepulse to command potentials from -70 to -10 mV was followed by a 200 ms pulse to 0 mV to measure the amount of inactivation. A single exponential of the same form as Eq. 1 was used to fit the current response to the 30 mV voltage command and extrapolated back to the start of the pulse. B was equal to 1 minus the extrapolated current divided by the current at -30 mV.

I_{NaP} current traces were fit with the following double-exponential equation:

$$f(t) = A\left(1 - e^{\frac{-t}{0.04}}\right)\left(1 - 0.5\left(1 - e^{\frac{-t}{s}}\right)\right) \tag{5}$$

where A is the maximum activation and limited to between 0 and -30 nA. The value 0.04 is the activation time constant. Initial fittings indicated that the amount of inactivation was approximately 0.5 for all three neurons in the range of potentials used to measure I_{NaP} so we fixed the value to 0.5 for simplification and reduce the degrees of freedom of the fitting algorithm. s is the inactivation time constant limited to values between 0.2 and 5 s.

Computational model

Conductance-based models for B51, B64, and B8 were generated and simulations conducted with the Simulator for Neural Networks and Action Potentials (SNNAP, version 8.1; Baxter and Byrne 2007). The three neurons were modeled as isolated compartments with no synaptic (electrical or chemical) connections between them. The membrane potential was determined by the following differential equation:

$$\frac{dV_i}{dt} = \frac{I_{Stim} - \sum_{j=1}^{m} Ivd_{ij}}{Cm_i} \tag{6}$$

where Cm_i is the membrane capacitance, I_{Stim} is the extrinsic stimulus current, Ivd_{ij} denotes voltage dependent current. Each voltage dependent current was determined by the following equation:

$$Ivd_{ij} = \left(\overline{g}vd_{ij}\right)A_{ij}^{p}B_{ij}\left(V_i - E_{ij}\right)f(BR) \tag{7}$$

where gvd_{ij} is the maximum conductance, A_{ij} represents the voltage and time dependent activation, B the voltage and time dependent inactivation, V_i the membrane potential, and E_{ij} the equilibrium potential. $f(BR)$ denotes regulation by a Ca^{2+} ion pool. I_{KCa} is regulated by two Ca^{2+} pools. The first Ca^{2+} pool that regulates I_{KCa} represents a constant occupied

Ca^{2+} binding site of I_{KCa} and its regulation is constant at 0.4. The second Ca^{2+} pool is filled by voltage-gated Ca^{2+} channels. This pool's regulation of I_{KCa} is determined by the following equations:

$$f(BR) = 1 + BR \tag{8}$$

$$\frac{dBR}{dt} = \frac{[Ca^{2+}] - BR}{0.1} \tag{9}$$

Where 0.1 is the time constant. The concentration of Ca^{2+} is determined by the following equation.

$$\frac{d[Ca^{2+}]}{dt} = 0.03(5(Ivd_{CaL} + Ivd_{CaR}) - [Ca^{2+}]) \tag{10}$$

The activation A_{ij} is determined by the following Boltzmann-type equations:

$$\frac{dA}{dt} = \frac{A_\infty - A}{\tau_A} \tag{11}$$

$$A_\infty = \frac{1}{\left(1 + e^{\frac{(h-V)}{s}}\right)^p} \tag{12}$$

where A is the level of activation, h is the voltage of the inflection point (half-activation), V is the voltage, and s is the slope parameter. We used a Matlab curve fitting algorithm to estimate the parameters for this equation. The maximum current (A in Eqs. 1-5) was converted to conductance using Ohm's law. The reversal potentials were -70 mV for I_A and I_D , -80 mV for I_{KCa}, and 60 mV for I_{CaL}, I_{CaR}, I_{Na} and I_{NaP}. To obtain the activation level, the conductance values at each potential were normalized to the maximum conductance of all membrane potentials measured for that cell. The activation data for each cell was fit with Eq. 12 (solid diamonds, solid lines in Figs. 2E, 2O, 3G, 4E, 4O, and

5G). For the voltage-gated Ca^{2+} channels, h was limited to between -50 and 10 mV and s was limited to between 0 and 20.

For the activation time constant:

$$\tau_A = \frac{\tau_{max} - \tau_{min}}{\left(1 + e^{\frac{(V - h_1)}{s_1}}\right)\left(1 + e^{\frac{(V - h_2)}{s_2}}\right)} + \tau_{min} \tag{13}$$

Where V is the voltage, $h_{1,2}$ determine the voltage of the inflection points, $s_{1,2}$ are slope parameters, τ_{max} is the maximum time constant, τ_{min} is the minimum time constant. For simplification and to aid in curve fitting of the current traces, the activation time constants of I_D and I_{NaP} were fixed to a single value, I_D was fixed to 0.01 s and I_{NaP} was fixed to 0.04 s. For voltage-gated Ca^{2+} channels, the activation time constants depended on the voltage clamp potential. To incorporate this voltage dependence into the model, the activation time constants were fit by hand with Eq. 13. The shapes of these curves in comparison to the time constant measurements are provided in Supplemental Fig. 2. For I_A (see Supplemental Fig. 3), the parameters for voltage dependency of activation were set to: B51, τ_{max} = 0.03 s, τ_{min} = 0.001 s, h = -30 mV, s = -5.7; B64, τ_{max} = 0.02 s, τ_{min} = 0.002 s, h = -20 mV, s = 5.7; B8, τ_{max} = 0.025 s, τ_{min} = 0.007 s, h_1 = -20 mV, s_1 = 6.

The inactivation, B_{ij} (Eq. 7), was defined by the following equations:

$$\frac{dB}{dt} = \frac{B_\infty - B}{\tau_B} \tag{14}$$

$$B_\infty = \frac{1 - B_{min}}{\left(1 + e^{\frac{(h - V)}{s}}\right)^p} + B_{min} \tag{15}$$

$$\tau_B = \frac{\tau_{max} - \tau_{min}}{\left(1 + e^{\frac{(V-h_1)}{s_1}}\right)\left(1 + e^{\frac{(V-h_2)}{s_2}}\right)} + \tau_{min} \tag{16}$$

where V is the voltage, $h_{1,2}$ determine the voltage of the inflection points, $s_{1,2}$ are slope parameters, τ_{max} is the maximum time constant, τ_{min} is the minimum time constant. The level of inactivation (Supplemental Fig. 1) for each measured potential was fit with Eq. 15. For I_A and voltage-gated Ca^{2+} channels, B_{min} was fixed at 0. For voltage-gated Ca^{2+} channels, h was limited to negative voltages. The inactivation time constant was estimated by s in the exponential decay terms in Eq. 1–5. There didn't appear to be any voltage dependence in inactivation time constants for I_A and I_{CaL} so the means of the inactivation time constants for all potentials were compared between the neurons (Supplementary Fig. 2A,D). There did appear to be voltage-dependence in the inactivation time constants for I_D, I_{CaR}, I_{NaP}. For I_D and I_{CaR}, the voltage dependence of the inactivation time constant seemed to be best fit by a sigmoidal equation and so the second term in the denominator of Eq. 16 was not included. The voltage dependence of inactivation time constants of I_{NaP} was fit using Eq. 16. The voltage dependence of inactivation time constants were fit by hand for I_D, I_{CaR}, and I_{NaP}.

In SNNAP, a voltage-clamp experiment was simulated with the exact protocol as experimental procedures. The resulting simulated current response was then compared to empirical data obtained from the recordings (Supplementary Fig. 3). The parameters in Eqs. 12-13,15-16 and $\bar{g}vd_{ij}$ in Eq.7 were adjusted slightly to provide the best fit for the current trace and the voltage dependence of the time constants in Supplementary Fig. 2. This study did not characterize Na^+-fast (I_{Na}), so the model for this channel was guided

by data of its characterization in *Aplysia californica* pedal neurons (Gilly et al., 1997) and was identical for all three neuron models.

Statistical analyses

Matlab was used for all statistical analyses. For all comparisons P values < 0.05 were considered to be significantly different. A Lilliefors goodness-of-fit test was used to test for normality of the distribution. Non-parametric tests were used when normality could not be assumed. The Student's t-test was used for comparing two groups and multiple groups were compared using ANOVA or Kruskal-Wallis test with the Tukey-Kramer post-hoc test.

REFERENCES

Bittner KC, Milstein AD, Grienberger C, Romani S, Magee JC (2017) Behavioral time scale synaptic plasticity underlies CA1 place fields. Science 357:1033-1036. PMCID: PMC7289271.

Broicher T, Kanyshkova T, Landgraf P, Rankovic V, Meuth P, Meuth SG, Pape HC, Budde T (2007) Specific expression of low-voltage-activated calcium channel isoforms and splice variants in thalamic local circuit interneurons. Mol Cell Neurosci 36:132-45. PMID: 17707654.

Canavier CC, Clark JW, Byrne JH (1991) Simulation of the bursting activity of neuron R15 in Aplysia: role of ionic currents, calcium balance, and modulatory transmitters. J Neurophysiol 66:2107-24. PMID: 1725879.

Canavier CC, Baxter DA, Clark JW, Byrne JH (1993) Nonlinear dynamics in a model neuron provide a novel mechanism for transient synaptic inputs to produce long-term alterations of postsynaptic activity. J Neurophysiol 69:2252-7. PMID: 8350142.

Canavier CC, Baxter DA, Clark JW, Byrne JH (1994) Multiple modes of activity in a model neuron suggest a novel mechanism for the effects of neuromodulators. J Neurophysiol 72:872-82. PMID: 7983542.

Carrasquillo Y, Burkhalter A, Nerbonne JM (2012) A-type K^+ channels encoded by Kv4.2, Kv4.3, and Kv1.4 differentially regulate intrinsic excitability of cortical pyramidal neurons. J Physiol 590:3877-3890. PMCID: PMC3476638.

Carrillo-Reid L, Tecuapetla F, Vautrelle N, Hernández A, Vergara R, Galarraga E, Bargas J (2009) Muscarinic enhancement of persistent sodium current synchronizes striatal medium spiny neurons. J Neurophysiol 102:682-90. PMID: 19474176.

Del Negro CA, Koshiya N, Butera RJ Jr, Smith JC (2002) Persistent sodium current, membrane properties and bursting behavior of pre-bötzinger complex inspiratory neurons in vitro. J Neurophysiol 88:2242-50. PMID: 12424266.

Derjean D, Bertrand S, Le Masson G, Landry M, Morisset V, Nagy F (2003) Dynamic balance of metabotropic inputs causes dorsal horn neurons to switch functional states. Nat Neurosci 6:274-81. PMID: 12592405.

Duncan PJ, Shipston MJ (2016) BK Channels and the Control of the Pituitary. Int Rev Neurobiol 128:343-68. PMID: 27238268.

Gilly WF, Gillette R, McFarlane M (1997) Fast and slow activation kinetics of voltage-gated sodium channels in molluscan neurons. J Neurophysiol 77:2373-84. PMID: 9163364.

Jangsangthong W, Kuzmenkina E, Khan IF, Matthes J, Hullin R, Herzig S (2010) Inactivation of L-type calcium channels is determined by the length of the N-terminaus of mutant beta(1) subunits. Pflugers Arch 459:399-411. PMID 19821165

Katz E, Stoler O, Scheller A, Khrapunsky Y, Goebbels S, Kirchhoff F, Gutnick MJ, Wolf F, Fleidervish IA (2018) Role of sodium channel subtype in action potential generation by neocortical pyramidal neurons. Proc Natl Acad Sci U S A 115:E7184-E7192. PMCID: PMC6065046.

Lorenzetti FD, Baxter DA, Byrne JH (2008) Molecular mechanisms underlying a cellular analog of operant reward learning. Neuron 59:815-828. PMCID: PMC2603610.

Metz AE, Jarsky T, Martina M, Spruston N (2005) R-type calcium channels contribute to afterdepolarization and bursting in hippocampal CA1 pyramidal neurons. J Neurosci. 25:5763-73 PMCID: PMC6724888.

Momohara Y, Neveu CL, Chen HM, Baxter DA, Byrne JH (2022) Specific plasticity loci and their synergism mediate operant conditioning. J Neurosci, in press. PMID: 34992131.

Mozzachiodi R, Lorenzetti FD, Baxter DA, Byrne JH (2008) Changes in neuronal excitability serve as a mechanism of long-term memory for operant conditioning. Nat Neurosci 11:1146-1148. PMCID: PMC5003050.

Nargeot R, Baxter DA, Byrne JH (1999a) In *vitro* analog of operant conditioning in *Aplysia*. I. Contingent reinforcement modifies the functional dynamics of an identified neuron. J Neurosci 19:2247-2260.

Nargeot R, Baxter DA, Byrne JH (1999b) In *vitro* analog of operant conditioning in *Aplysia*. II. Modifications of the functional dynamics of an identified neuron contribute to motor pattern selection. J Neurosci 19:2261-2272.

Pennartz CM, Bierlaagh MA, Geurtsen AM (1997) Cellular mechanisms underlying spontaneous firing in rat suprachiasmatic nucleus: involvement of a slowly inactivating component of sodium current. J Neurophysiol 78:1811-25. PMID: 9325350.

Plotkin JL, Day M, Surmeier DJ (2011) Synaptically driven state transitions in distal dendrites of striatal spiny neurons. Nat Neurosci 14:881-8. PMCID: PMC3235762.

Plummer MR, Kirk MD (1990) Premotor neurons B51 and B52 in the buccal ganglia of *Aplysia californica*: synaptic connections, effects on ongoing motor rhythms, and peptide modulation. J Neurophysiol 63:539-558.

Randall AD, Tsien RW (1997) Contrasting biophysical and pharmacological properties of T-type and R-type calcium channels. Neuropharmacology 36:879-893. PMID: 9257934.

Tsuk S, Michaelevski I, Bentley GN, Joho RH, Chikvashvili D, Lotan I. (2005) Kv2.1 channel activation and inactivation is influenced by physical interactions of both syntaxin 1A and the syntaxin 1A/soluble N-ethylmaleimide-sensitive factor-25 (t-SNARE) complex with the C terminus of the channel. Mol Pharmacol 67:480-8. PMID: 15525758.

Yuan W, Burkhalter A, Nerbonne JM (2005) Functional role of the fast transient outward K+ current IA in pyramidal neurons in (rat) primary visual cortex. 25:9185-9194. PMC6725755.